

Buckling and Pull-In Instability of Multi-Walled Carbon Nanotube Probes Near Graphite Sheets Using Power Series and Padé Approximants

Jalal Alsarraf*, Majed A. Alwatheeqi**, Esam A.M. Husain*, Khaled Alawadhi*

*(Automotive and Marine Engineering Technology Department, Public Authority for Applied Education and Training, Shuwaikh 70654)

** (Industrial Training Institute – Shuwaikh, Public Authority for Applied Education and Training, Shuwaikh 70654)

ABSTRACT

In this paper, integration of the power series method and the Padé approximants (PS-Padé) is utilized to study buckling and pull-in instability of multi-walled carbon nanotube (MWCNT) cantilevers in the vicinity of graphite sheets due to intermolecular forces. A hybrid nano-scale continuum model based on the Lennard–Jones potential is used to simulate the Van der Waals forces and evaluate the buckling of MWCNT. A closed form power series, based on the symbolic power series polynomials, is utilized to obtain a series solution for the governing boundary value differential equation of the nanotube. In order to handle the boundary conditions and increasing the accuracy of solution, the symbolic power series are transformed into Padé approximants. The governing differential equation is also solved numerically using the finite difference method. The PS-Padé results are compared with the numerical results and other methods reported in literature. The results obtained by using the PS-Padé approach correspond very well with the numerical results. Furthermore, the detachment length and the minimum gap between MWCNT and the graphite plane as important parameters of engineering designs are computed. It is found that for a fixed gap, the detachment length of a MWCNT can be increased with the increase of the radius, wall thickness and the effective Young modulus of the MWCNT.

Keywords - Cantilever, MWCNT, Padé, Pull-in instability, Symbolic power series.

I. Introduction

Multi-walled Carbon Nanotubes (MWCNTs) are types of nano-materials with outstanding mechanical properties. Nowadays, MWCNTs have attracted considerable attention because of their unique mechanical and chemical properties. These novel materials can be visualized in the form of nano-scale concentric cylinders rolled up by graphene sheets. There are numerous reports on the fabrication of single-walled carbon nanotubes (SWCNT) and MWCNT probes [1]-[3]. MWCNTs can be synthesized by different techniques, including laccase-mediator [4], situ oxidative polymerization method [5]-[7]. Single-walled and multi-walled carbon nanotubes have been utilized as electrochemical sensors [8], catalysts [9], [10], structures [11], and Atomic force microscopes (AFM) [12]. Electrically induced static and dynamic mechanical buckling and pull-in instability of MWCNT cantilevers have many applications, such as nanotube based electromechanical system (NEMS) switches [12]-[14].

Consider a typical MWCNT cantilever probe/switch suspended above a graphite surface

with a small gap between them. When the size of the gap decreases to nanometers, the Van der Waals interaction buckles the MWCNT to the substrate. In a recent piece of work [15], the authors utilized a hybrid continuum model to consider the molecular force-induced buckling of the cantilever freestanding MWCNT probes/actuators suspended over graphite sheets. They carried out the governing equation of the deflection of MWCNT cantilever probes/actuators in the vicinity of thin and thick graphite layers. The governing equation of the hybrid distributed model leads to a fourth-order nonlinear, ordinary differential equation. Because of the nonlinearity of the governing equation of the distributed model, an exact solution does not yet exist.

Reference [15] used the Green's function method with a simple second order polynomial as the shape function to obtain deflection and pull-in parameters of MWCNT cantilevers. They have also used the Adomian decomposition method (ADM) to obtain pull-in instability of MWCNT cantilevers. However, the accuracy of the results of the Green's method and the Adomian decomposition method [15] for calculating deflection of MWCNT cantilevers near

the pull-in instability is not perfect. Reference [16] examined a monotone positive solution to obtain a resolution for the buckling of MWCNTs. The monotone solution is a comparatively accurate solution for low values of intermolecular forces, but it fails to evaluate the pull-in instability of MWCNT cantilevers.

The combination of any series solutions with the Padé approximants provides a powerful tool for increasing the accuracy of boundary value problems [17]-[19]. Hence, the accuracy of the series methods can be enhanced by using Padé approximants.

In this study, in order to obtain an accurate analytical solution for pull-in instability of MWCNTs in the vicinity of graphite sheets, integration of symbolic power series with Padé approximants (PS-Padé) is used as a new approach to study the buckling and pull-in instability of MWCNT cantilever actuators. A fair comparison is made between the method presented and numerical results as well as between the Adomian decomposition method and monotone solution reported in literature.

II. Mathematical Model

Fig. 1 shows a physical schematic of a typical MWCNT cantilever near a surface consisting of N graphene layers, with interlayer distance d . The length of MWCNT is L , the mean radius value is R_w , the number of walls of nanotube is N_w , and the gap between MWCNT and the graphite surface is D .

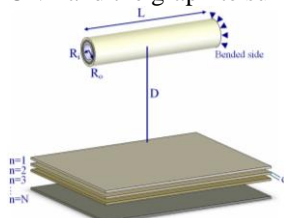


Fig. 1 Schematic of a MWCNT cantilever in the vicinity of graphite sheets

Based on continuum mechanics, a MWCNT is modeled by concentric cylindrical tubes. E is the Young's modulus of MWCNT which typically is in the range of 0.9 to 1.2 TPa, and the cross-sectional moment of inertia I is equal to $\pi (R_o^4 - R_i^4)/4$ [15]. By neglecting the effect of large displacement (finite kinematics) for $L/D_e > 10$ and applying the Euler theory [20], [21], the governing equation of a MWCNT cantilever can be written as the following boundary value ordinary differential equation [15]:

$$E_{eff} I \frac{d^4 U}{dX^4} = q_{w dv} (D - U) \quad (1-a)$$

subject to the following geometrical boundary conditions at fixed end:

$$U(0) = \frac{dU}{dX}(0) = 0 \quad (1-b)$$

and, natural boundary conditions at free end, as follows:

$$\frac{d^2 U}{dX^2}(L) = \frac{d^3 U}{dX^3}(L) = 0 \quad (1-c)$$

where X is the position along MWCNT measured from the bending side, U is the deflection of MWCNT cantilever and $q_{w dv}$ is the intermolecular force per unit length of MWCNT. According to the work of [15], $q_{w dv}$ can be represented as follows:

$$q_{w dv} = \begin{cases} \frac{C_6 \sigma^2 \pi^2 N_w R_w}{d(D-U)^4} & \text{For large number of layers} \\ \frac{4C_6 \sigma^2 \pi^2 N N_w R_w}{d(D-U + Nd/2)^4} & \text{For small number of layers} \end{cases} \quad (2)$$

In (2), $\sigma \approx 38 \text{ nm}^{-2}$ [22] is the graphene surface density and $C_6 = 15.2 \text{ eV } \text{ \AA}^6$ is the attractive constants for the carbon-carbon interaction [23]. By substituting (2) in (1) and using the following substitutions:

$$x = \frac{X}{L}, \quad u = \begin{cases} \frac{U}{D} & (n=4) \\ \frac{U}{D + Nd/2} & (n=5) \end{cases} \quad (3-a)$$

and:

$$f_n = \begin{cases} \frac{C_6 \sigma^2 \pi^2 N_w R_w L^4}{d E_{eff} I D^5} & (n=4) \\ \frac{4C_6 \sigma^2 \pi^2 N N_w R_w L^4}{E_{eff} I (D + Nd/2)^6} & (n=5) \end{cases} \quad (3-b)$$

the dimensionless form of (1) can be obtained as follows:

$$\frac{d^4 u}{dx^4} = \frac{f_n}{(1-u(x))^n} \quad (4-a)$$

$$u(0) = u'(0), \quad \text{at } x=0, \quad (4-b)$$

$$u''(1) = u'''(1) = 0, \quad \text{at } x=1 \quad (4-c)$$

In the following text, $n=4$ and $n=5$ correspond to the large number and small number of graphene layers, accordingly. In the equations, prime denotes differentiation with respect to non-dimensional length of x .

III. Analytical Solution

Equation (4-a) subject to (4-b) and (4-c) can be solved using a symbolic power series enhanced with Padé approximants. The basic idea of the symbolic power series method and Padé approximants are explained in the works of [17], [18] and also [24], [25].

III.1 Symbolic Power Series Method

Based on the symbolic power series method, the fourth-order differential equation of (4-a) can be written as a system of four first order differential equation, as follows:

$$\begin{aligned} \frac{du_1(x)}{dx} &= u_2(x) \\ \frac{du_2(x)}{dx} &= u_3(x) \\ \frac{du_3(x)}{dx} &= u_4(x) \\ \frac{du_4(x)}{dx} &= \frac{f_n}{(1-u_1(x))^n} \end{aligned} \quad (5)$$

subject to the following boundary conditions:

$$\begin{aligned} u_1(0) &= 0, & u_2(0) &= 0, \\ u_3(0) &= P, & u_4(0) &= Q \end{aligned} \quad (6)$$

and to the constraints which come from (4-c):

$$u_3(1) = 0, \quad u_4(0) = 0, \quad (7)$$

Here, P and Q are constants which later will be computed from the boundary conditions, (4-c) or (7). Based on the method of symbolic power series introduced by [17], [18], the solution procedure is started as follows:

$$\begin{aligned} u_1(x) &= 0 + e_1 \\ u_2(x) &= 0 + e_2 \\ u_3(x) &= P + e_3 \\ u_4(x) &= f_n + e_4 \end{aligned} \quad (8)$$

Substituting (8) in (5) and neglecting higher order terms yields:

$$\begin{aligned} e_1 + 0 &= 0, \\ e_2 - P &= 0, \\ e_3 - Q &= 0, \\ e_4 - f_n &= 0, \end{aligned} \quad (9)$$

Solving (9) for e_1 to e_4 and substituting the obtained values into (8) and considering a higher term gives the first approximation of the solution as:

$$\begin{aligned} u_1(x) &= 0 + e_1 x^2 \\ u_2(x) &= Px + e_2 x^2 \\ u_3(x) &= P + Qx + e_3 x^2 \\ u_4(x) &= Q + f_n x + e_4 x^2 \end{aligned} \quad (10)$$

Again, substituting (10) in (5) and neglecting higher order terms yields:

$$\begin{aligned} P - 2e_1 &= 0, \\ Q - 2e_2 &= 0, \\ 2e_3 - f_n &= 0, \\ 2e_4 &= 0, \end{aligned} \quad (11)$$

Substituting the new values of e_1 to e_4 into (10) and considering a higher term results in:

$$\begin{aligned} u_1(x) &= \frac{P}{2} x^2 + e_1 x^3 \\ u_2(x) &= \frac{Q}{2} x^2 + Px + e_2 x^3, \\ u_3(x) &= \frac{f_n}{2} x^2 + Qx + P + e_3 x^3 \\ u_4(x) &= Q + f_n x + e_4 x^3 \end{aligned} \quad (12)$$

By substituting e_1 to e_4 in (5) and repeating this procedure, the following power series for u_1 is obtained after eight iterations:

$$u_1(x) = \frac{P}{2} x^2 + \frac{Q}{6} x^3 + \frac{f_n P}{24} x^4 + \frac{nf_n P}{720} x^5 + \frac{nf_n Q}{5040} x^6 + \left(\frac{n(n+1)f_n P^2}{13440} + \frac{nf_n^2}{40320} \right) x^8 + O(x^9) \quad (13)$$

Continuing this procedure results in a symbolic power series with higher terms. Here, undetermined coefficients, P and Q , correspond to the second and third derivatives of beam deflection with respect to x at $x = 0$, accordingly. These coefficients can be evaluated using natural boundary conditions at free end (i.e. $u_2(1) = 0$ and $u_3(1) = 0$).

The combination of any series solutions with the Padé approximation provides a powerful tool for handling initial or boundary value problems on infinite or semi-infinite domains [24]-[26]. In order to increase the accuracy of solution, the power series in the symbolic form and before computation of the unknown values of P and Q , can be converted to Padé approximation.

III.2 Padé Approximants

Any power series can be represented as a function $f(x)$, in the form of:

$$f(x) = \sum_{i=0}^{\infty} a_i x^i \quad (14)$$

where, the expansion of (14) is the fundamental starting point of any analysis using Padé approximants. The objective of the Padé approximants is to seek a rational function for the series. The Padé approximants converge on the entire real axis if the series solution is free of singularities on the real axis [24]. A Padé approximant is a rational fraction which provides us with more stable expression than the original power series. The notation for such a Padé approximant can be defined as per [26]:

$$a_0 + a_1 \eta + a_2 \eta^2 + \dots = \frac{p_0 + p_1 \eta + p_2 \eta^2 + \dots + p_M \eta^M}{1 + q_1 \eta + q_2 \eta^2 + \dots + q_L \eta^L} \quad (15)$$

Both sides of (14) are multiplied by the denominator of the right-hand side of (15):

$$\begin{aligned} a_0 + (a_1 + a_0 q_1) \eta + (a_2 + a_1 q_1 + a_0 q_2) \eta^2 + \dots + (a_3 + \sum_{k=1}^3 a_{1-k} q_k) \eta^3 + \dots + (a_M + \sum_{k=1}^M a_{M-k} q_k) \eta^M + \dots \\ + (a_{M+L} + \sum_{k=1}^L a_{M-k} q_k) \eta^{M+L} = p_0 + p_1 \eta + p_2 \eta^2 + \dots + p_M \eta^M + 0 \end{aligned} \quad (16)$$

By comparing the coefficients of both sides of (16), one can find that:

$$a_l + \sum_{k=1}^M a_{l-k} q_k = p_l, \quad l=0, \dots, M \quad (17)$$

$$a_l + \sum_{k=1}^L a_{l-k} q_k = 0, \quad l=M+1, \dots, M+L \quad (18)$$

M and L are the degrees of numerator and denominator in the Padé series, respectively. By solving the linear equation, (18), the q_k ($k=1, \dots, L$) is determined. After that, by substituting q_k in (17), p_l ($l=0, \dots, M$) will be determined. For instance, by following this procedure, the Padé series of (13) with the size of {2, 2} for u_l , can be obtained as follows.

From (18) with $L=2$ and $M=2$:

$$\begin{cases} a_3 + a_2 q_1 + a_1 q_2 = 0 \\ a_4 + a_3 q_1 + a_2 q_2 = 0 \end{cases} \quad (19)$$

Solving for q_1 and q_2 :

$$q_1 = \frac{a_2 a_3 - a_1 a_4}{a_1 a_3 - a_2^2}, \quad q_2 = \frac{a_2 a_4 - a_3^2}{a_1 a_3 - a_2^2} \quad (20)$$

From (17) with $M=2$:

$$\begin{cases} p_0 = a_0 \\ p_1 = a_1 + a_0 q_1 \\ p_2 = a_2 + a_1 q_1 + a_0 q_2 \end{cases} \quad (21)$$

After substituting the obtained coefficients and simplification, the Padé series of u_l with the size of {2, 2} is as follows:

$$u_1(x) = \frac{3}{2} \frac{P^3 x^2}{3P^2 - QPx + \left(-\frac{1}{4} f_n P + \frac{1}{3} Q^2\right) x^2} \quad (22)$$

If the order of Padé approximation increases, the accuracy of the solution increases [25], [26].

IV. Results and Discussion

In order to verify the convergence of Padé approximants, deflection of a typical nanotube-actuator, which is used in the work of [15], is computed analytically using the symbolic power series method. Then the power series are converted to Padé approximants. The solution results are compared with the numerical results as well as the monotone method [16], the Green's method and Adomian decomposition method [15]. Numerical results are obtained using the finite difference method based on collocation points and Newton's method [27], [28]. A highly accurate solution with a relative tolerance of 10^{-8} is achieved. Table 1 and Table 2 compare MWCNT cantilever tip deflection (u_{tip}), computed using different terms of symbolic power series and different sizes of Padé approximants, respectively. These tables ensure the convergence and accuracy of the power series and Padé approximants. Table 2 reveals that higher accuracy can be obtained by evaluating more terms of the Padé approximants.

The relative error is computed from:

$$Error = \left| \frac{u_{Analytical} - u_{Numerical}}{u_{Numerical}} \right| \quad (23)$$

where, $u_{Analytical}$ and $u_{Numerical}$ are the MWCNT cantilever tip deflection, computed from the analytical method (i.e. PS or PS-Padé) and the tip deflection computed using numerical method, respectively. The *Error* represents the relative error.

Table 1

The Evaluated Tip Deflection of a Typical MWCNT Cantilever Using Different Terms of PS Method for $f_n=0.5$

Series Size	Tip Deflection PS, n=4	Error n=4	Tip Deflection PS, n=5	Error n=5
4	0.06250	1.903E-01	0.06250	2.491E-01
5	0.06250	1.903E-01	0.06250	2.491E-01
6	0.08657	1.215E-01	0.09533	1.453E-01
7	0.07215	6.525E-02	0.07516	9.700E-02
8	0.08228	6.592E-02	0.09350	1.233E-01
9	0.07396	4.190E-02	0.07737	7.046E-02
10	0.07946	2.945E-02	0.08842	6.228E-02
11	0.07564	2.015E-02	0.07983	4.087E-02
12	0.07833	1.476E-02	0.08613	3.479E-02
13	0.07646	9.511E-03	0.08137	2.236E-02
14	0.07772	6.816E-03	0.08475	1.826E-02
15	0.07684	4.494E-03	0.08223	1.211E-02
16	0.07743	3.087E-03	0.08400	9.263E-03
Numerical		0.077192		0.083233676

Table 2

The Evaluated Tip Deflection of a Typical MWCNT Cantilever Using Different Terms of PS-Padé for $f_n=0.5$

Padé Size	Tip Deflection PS-Padé, (n=4)	Error (n=4)	Tip Deflection PS-Padé, (n=5)	Error (n=5)
{2,2}	0.07368	4.544E-02	0.07405	1.103E-01
{3,3}	0.07525	2.519E-02	0.08009	3.777E-02
{4,4}	0.07724	5.716E-04	0.08344	2.449E-03
{5,5}	0.07710	1.148E-03	0.08353	3.504E-03
{6,6}	0.07719	1.795E-05	0.08323	3.415E-05
{7,7}	0.07719	2.054E-06	0.08323	4.200E-06
{8,8}	0.07719	9.067E-07	0.08324	2.537E-05
{9,9}	0.07719	1.460E-08	0.08323	5.240E-08
Numerical		0.0771924		0.0832336

The results in Table 2 show the relative error between analytical and numerical results is less than 0.0034% by selecting PS- Padé size of {6,6}. It is worth noticing that the Padé approximants with size {6,6} are obtained from 15 terms of power series (i.e. $O(x^{16})$). Comparing this error with the same series size of the PS method (i.e. 15 terms and relative error of 1.2%), shows the PS- Padé method could compute deflection of MWCNT cantilever with more accuracy than the PS method. The results of PS- Padé with size of {6, 6} with 0.0034% error are very similar to the numerical results. Therefore, the Padé size of {6, 6} is selected, for convenience.

IV.1 Instability Study

In order to study pull-in instability of multi-wall carbon nanotube cantilevers, (4) is solved

numerically simulated and the results are compared with the results of the PS-Padé method. The results show that for f_n greater than critical value of intermolecular force (f_n^*), a numerical solution does not exist and the MWCNT collapses on to the sheets. The pull-in value of MWCNT-graphite attraction and the MWCNT pull-in tip deflection can also be evaluated using the PS-Padé technique by setting $du(1)/df_n \rightarrow \infty$ in the solution.

The relationship between f_n and u_{tip} are presented in Figs. 2 and 3 for large and small numbers of graphene layers. Fig. 3 depicts the non-dimensional tip deflection of MWCNT which it increases from zero to pull-in instability as f_n raises from zero to f_n^* . Table 3 compares the obtained values of f_n^* using different methods for large and small numbers of graphene layers. When intermolecular attraction exceeds the critical value of f_n^* , no solution exists and the instability occurs.

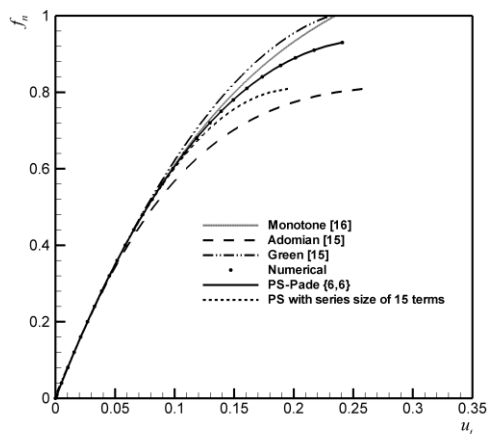


Fig. 2 Relation between f_n and MWCNT cantilever tip deflection in the vicinity of large number of graphene layers ($n=4$)

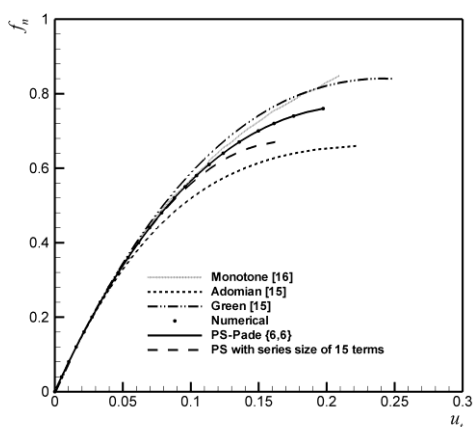


Fig. 3 Relation between f_n and MWCNT cantilever tip deflection in the vicinity of small number of graphene layers ($n=5$)

Table 3
 Comparison of f_n^* obtained by different methods

Model	f_n^* ($n=4$)	error ($n=4$)	f_n^* ($n=5$)	error ($n=5$)
Numerical Solution	0.939	-	0.769	-
Monotone	-	-	-	-
Green's Function	1.025	9.2	0.841	9.4
Adomian method	0.814	13.3	0.661	14
PS 15 terms of series	0.810	13.7	0.670	12.9
PS Padé {6,6}	0.939	0	0.769	0

The results in Figs. 2 and 3 and Table 3 reveal that the PS-Padé method is more accurate than other methods in comparison with the numerical results. The centerline deflection of a typical MWCNT under intermolecular force for a large number of graphene layers and a small number of graphene layers are shown in Fig. 4 and Fig. 5, respectively.

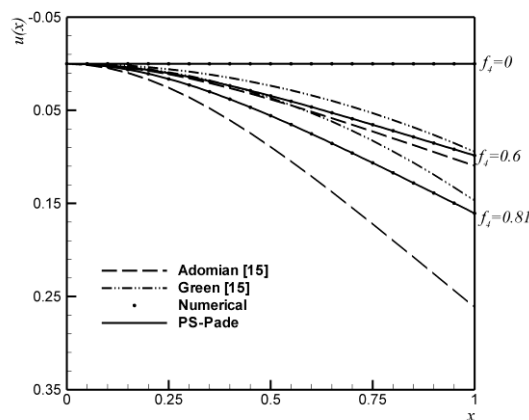


Fig. 4 Center line buckling of MWCNT for different values of f_n when $n=4$

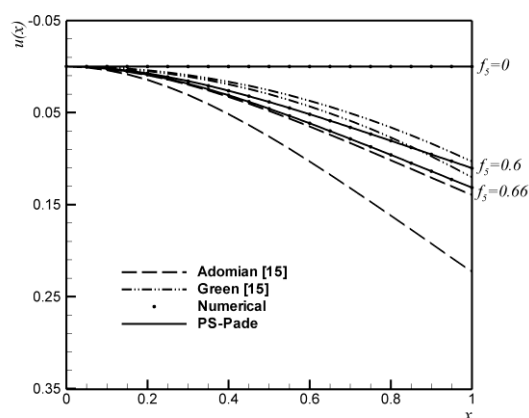


Fig. 5 Center line buckling of MWCNT for different values of f_n when $n=5$

These figures compare the PS-Padé results with the numerical results as well as with Green's function method and the Adomian method [15]. The obtained PS-Padé solution at the onset of pull-in

instability for the large number of graphene layers (i.e. $n=4$) is as follows:

$$u^{(4)} = \frac{(5322605345000x^2 + 1658444884000x^3 - 234805234000x^4 + 69078875300x^5 + 290980676200x^6)}{(10901369930000 + 933512630000x - 571657749500x^2 - 920411794500x^3 + 25098037920x^4 + 16516697530x^5 + 4129243874x^6)} \quad (24)$$

The PS-Padé solution at the onset of instability for the small number of graphene layers is:

$$u^{(3)} = \frac{(4449476518000x^2 + 1100463496000x^3 - 1906546258000x^4 + 151168135800x^5 + 208062912800x^6)}{(10976849700000 + 8699010750000x - 828753282000x^2 - 766502257000x^3 + 43693697980x^4 + 18891227440x^5 + 4867875469x^6)} \quad (25)$$

When the gap between the plane and the suspended nanotube is small enough, the nanotube may collapse on to the graphite sheets without applying voltage due to the intermolecular attractions. The stable length is an important parameter for design of nano-switches or AFM probes and some other engineering applications [12]-[14]. By substituting the obtained value of f_n^* at the onset of instability in definition of f_n (i.e. (3-b)), then solving for corresponding minimum gap (D_{min}) and detachment length (L_{max}) of freestanding MWCNT, the following relations are obtained:

$$L_{max} = \begin{cases} \sqrt[4]{\frac{0.939dEtR_w^2 D^5}{C_6\sigma^2\pi N_w}} & \text{for } n = 4 \\ \sqrt[4]{\frac{0.192EtR_w^2 (D + Nd/2)^6}{C_6\sigma^2\pi NN_w}} & \text{for } n = 5 \end{cases} \quad (26)$$

$$D_{max} = \begin{cases} \sqrt[5]{\frac{1.065 C_6\sigma^2\pi N_w L^4}{dEtR_w^2}} & \text{for } n = 4 \\ \sqrt[6]{\frac{5.201C_6\sigma^2\pi NN_w L^4}{EtR_w^2} - \frac{Nd}{2}} & \text{for } n = 5 \end{cases} \quad (27)$$

Equation (26) shows the detachment length of a MWCNT would increase with an increase of the radius, wall thickness or effective Young modulus of the MWCNT.

V. Conclusions

A mathematical model based on a nano-scale continuum model and the Lennard-Jones potential is used to study buckling of MWCNT cantilevers near the graphite sheets. The governing equation leads to a fourth-order ordinary differential equation. Then, integration of the Adomian decomposition method and the Padé approximants is used as a new accurate technique to obtain a solution for buckling of MWCNT cantilevers. The ADM-Padé solution is compared with the numerical method, Green's function, the Adomian solution and a symbolic power series in figures and tables. Comparison between the Adomian results and ADM-Padé results show that Padé approximants enhanced the convergence of Adomian decomposition polynomials to handling the governing boundary value problem near the pull-in area. Finally, by using the ADM-Padé technique, the critical value of Van der Waals attraction (f_n^*) and detachment length of MWCNT as basic parameters for design and

selecting components of nano-electro mechanical systems has been determined.

References

- [1] L. Wang, T. A. Stueckle, A. Mishra, R. Derk, T. Meighan, V. Castranova, and Y. Rojanasakul, Neoplastic-like transformation effect of single-walled and multi-walled carbon nanotubes compared to asbestos on human lung small airway epithelial cells, *Nanotoxicology*, 8(5), 2014, 485-507.
- [2] K. Saeed and I. Khan, Preparation and properties of single-walled carbon nanotubes/poly (butylene terephthalate) nanocomposites, *Iranian Polymer Journal*, 23(1), 2014, 53-58.
- [3] H. Zanin, E. Saito, H. J. Ceragioli, V. Baranauskas, and E. J. Corat, Reduced graphene oxide and vertically aligned carbon nanotubes superhydrophilic films for supercapacitors devices, *Materials Research Bulletin*, 49, 2014, 487-493.
- [4] G. Otrokho, D. Pankratov, G. Shumakovich, M. Khlupova, Y. Zeifman, I. Vasil'eva, and A. Yaropolov, Enzymatic synthesis of polyaniline/multi-walled carbon nanotube composite with core shell structure and its electrochemical characterization for supercapacitor application, *Electrochimica Acta*, 123, 2014, 151-157.
- [5] Z. Z. Zhu, G. C. Wang, M. Q. Sun, X. Y. Li, and C. Z. Li, Fabrication and electrochemical characterization of polyaniline nanorods modified with sulfonated carbon nanotubes for supercapacitor applications, *Electrochimica Acta*, 56(3), 2011, 1366-1372.
- [6] L. Fu and A. M. Yu, Carbon nanotubes based thin films: fabrication, characterization and applications, *Reviews on Advanced Materials Science*, 36, 2014, 40-61.
- [7] Q. Guo, D. Liu, X. Zhang, L. Li, H. Hou, O. Niwa, and T. You, Pd-Ni alloy Nanoparticle/Carbon Nanofiber Composites: Preparation, Structure, and Superior Electrocatalytic Properties for Sugar Analysis, *Analytical Chemistry*, 86, 2014, 5898-5905.
- [8] S. Ebrahim, R. El-Raey, A. Hefnawy, H. Ibrahim, M. Soliman, and T. M. Abdel-Fattah, Electrochemical sensor based on polyaniline nanofibers/single wall carbon nanotubes composite for detection of malathion, *Synthetic Metals*, 190, 2014, 13-19.
- [9] J. Safari and S. Gandomi-Ravandi, Silver decorated multi-walled carbon nanotubes as a heterogeneous catalyst in the sonication of 2-

- aryl-2, 3-dihydroquinazolin-4 (1 H)-ones, *RSC Advances*, 4(23), 2014, 11654-11660.
- [10] G. Wang, J. Wang, H. Wang, and J. Bai, Preparation and evaluation of molybdenum modified Fe/MgO catalysts for the production of single-walled carbon nanotubes and hydrogen-rich gas by ethanol decomposition, *Journal of Environmental Chemical Engineering*, 2(3), 2014, 1588-1595.
- [11] W. Lin and C. P. Wong, *U.S. Patent No. 8,702,897*, U.S. Patent and Trademark Office, Washington, DC, 2014.
- [12] M. C. Strus, A. Raman, C. S. Han, and C. V. Nguyen, Imaging artefacts in atomic force microscopy with carbon nanotube tips, *Nanotechnology*, 16, 2005, 2482–2492.
- [13] C. V. Nguyen, R. M. D. Stevens, J. Barber, J. Han, and M. Meyyappan, Carbon nanotube scanning probe for profiling of deep-ultraviolet and 193 nm photoresist patterns, *Applied Physics Letters*, 81(5), 2002, 901-903.
- [14] M. Paradise and T. Goswami, Carbon nanotubes–production and industrial applications, *Materials & Design*, 28(5), 2007, 1477–89.
- [15] A. Koochi, A. S. Kazemi, A. Noghrehabadi, A. Yekrangi, and M. Abadyan, New approach to model the buckling and stable length of multi walled carbon nanotube probes near graphite sheets, *Materials & Design*, 32(5), 2011, 2949–2955.
- [16] A. Noghrehabadi, M. Ghalambaz, and A. Ghanbarzadeh, Buckling of multi wall carbon nanotube cantilevers in the vicinity of graphite sheets using monotone positive method, *Journal of Computational and Applied Research in Mechanical Engineering*, 1(2), 2012, 89-97.
- [17] E. Celik and M. Bayram, Arbitrary order numerical method for solving differential-algebraic equation by Padé series, *Applied Mathematics and Computation*, 137, 2003, 57–65.
- [18] E. Celik and M. Bayram, The numerical solution of physical problems modeled as a system of differential-algebraic equations (DAEs), *Journal of the Franklin Institute*, 342, 2005, 1–6.
- [19] M. Ghalambaz, A. Noghrehabadi, M. Ghalambaz, M. Abadyan, Y. T. Beni, M. N. Abadi, and M. N. Abadi, A new solution for natural convection about a vertical cone embedded in porous media prescribed wall temperature using power series – Padé, *Procedia Engineering*, 10, 2011, 3749-3757.
- [20] R. C. Batra and A. Sears, Continuum models of multi-walled carbon nanotubes, *International Journal of Solids and Structures*, 44, 2007, 7577–7596.
- [21] C. F. Ke, H. D. Espinosa, and N. Pugno, Numerical analysis of nanotube based NEMS devices – part II: role of finite kinematics, *Journal of Applied Mechanics*, 72, 2005, 726–31.
- [22] M. Desquenes, S. V. Rotkin, and N. T. Alaru, Calculation of pull-in voltages for carbon-nanotube- based nanoelectromechanical switches, *Nanotechnology*, 13, 2002, 120–31.
- [23] L. A. Girifalco, M. Hodak, and R. S. Lee, Carbon nanotubes, buckyballs, ropes, and a universal graphitic potential, *Physical Review B*, 62,(19), 2000, 13104–13110.
- [24] H. Simsek, and E. Celik, The successive approximation method and Padé approximants for solutions the non-linear boundary value problem, *Applied Mathematics and Computation*, 146, 2003, 681–690.
- [25] A. M. Wazwaz, Analytical approximations and Padé approximations for Volterra’s population model, *Applied Mathematics and Computation*, 100, 1999, 13–25.
- [26] E. Celik and M. Bayram, On the numerical solution of differential-algebraic equations by Padé series, *Applied Mathematics and Computation*, 137, 2003, 151-160.
- [27] H. B. Keller, Numerical solution of two-point boundary value problems, *SIAM Regional Conference Series in Applied Mathematics*, Philadelphia, PA, 1976.
- [28] R. D. Russell and L. F. Shampine, A collocation method for boundary value problems, *Numerische Mathematik*, 19, 1972, 1-28.